

**Cloudy with a Chance of Snow:
The Life of a Snowflake in a Cloud Microphysics Model**

Rubaiyat Bin Islam, *Tulane University*

Anthony Chen, *University of Michigan*

Mona Khoshnevis, *Brown University*

Gitte Kremling, *University of Wisconsin*

Darsh Nathawani, *University at Buffalo*

Maria Onyido, *Auburn University*

Justin Swain, *University of North Texas*

Tobias Timofeyev, *University of Vermont*

Zengyan Zhang, *Utah State University*

Mentor: Valeria Barra, *California Institute of Technology*

Graduate Student Mathematical Modeling Camp (GSMMC 2022)

University of Delaware, June 08-11, 2022

Problem Statement:

Clouds can be very fascinating and romantic to stare at, but they provide great challenges from a mathematical and numerical modeling point of view. In fact, clouds currently are one of the greatest sources of uncertainty in climate forecasts. One of the reasons why they are so difficult to capture in current numerical models is the extreme range of scales involved: from processes happening on the length scales of individual cloud droplets, to the large scale eddies driving the air circulation of a cloudy field. It is important to keep track of the microscopic properties of cloud particles in order to properly resolve, for example, the physics of rain or snow formation. On the other hand, it is also very important to keep the simulation computationally affordable. How to make things simple without oversimplifying?

We will look at this question from the point of view of a snowflake. Snowflake crystals come in many different shapes and sizes. This can, in turn, affect their growth rates, collision rates and their sedimentation rates. Although these are all very important aspects to take into account, typically, current cloud models used in the climate and atmospheric science communities can only afford to predict cumulative quantities, such as the total mass of snow produced in a cloud.

This project will start by considering a simple, idealized model of the shape of a snowflake. Building upon this idealized model, we will then consider possible variations or extensions to make the model more realistic. The main goal for this workshop will be to come up with possible mathematical models that are detailed enough to capture the different possible snowflake shapes, but simple enough that they can be integrated into a more complex cloud model, and therefore be useful for climate predictions. Some additional questions that we could answer during this workshop can then help us build our understanding of how precipitation rates can be affected by different snowflake geometries, and how we could potentially include more complexity.

1 Introduction

Earth system modeling is of increasing relevance in our rapidly changing world. Earth system models are complex models that couple all the interacting systems that make up the Earth: the atmosphere, the oceans, terrestrial landmasses, rivers, the biosphere, sea ice, glaciers, and human behavior, among others. These models are how we model climate change decades and centuries into the future. However, because of the size of the Earth and the complexity of these models, there are limits on the resolution that these models can be run at. Climate models are generally run with grid cells on the order of 100 by 100 kilometers. However, these grid cells are far too large to capture many important processes which impact the atmosphere and oceans. These processes must be incorporated into earth system models via physical parametrizations.

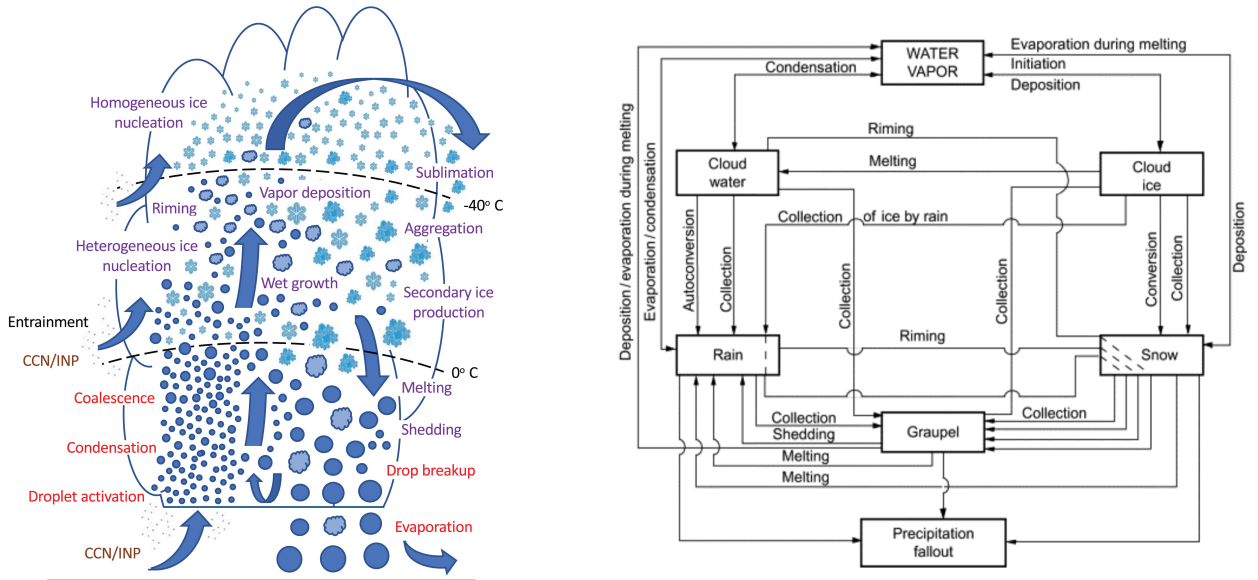


Figure 1: Left: Schematic depicting the physical processes happening in a cloud. Right: a flow chart representation of a cloud microphysics software package (often integrated in a larger climate model).

An example of a parametrized process is cloud microphysics. Clouds are immensely complicated, and actually modeling the inside of a cloud would require a significantly smaller grid size (see Figure 1). In order to incorporate cloud microphysics into earth system models, there are several different methods. Zero-th moment cloud microphysics considers only bulk quantities, and is the simplest, but also least accurate. First moment cloud microphysics considers the interactions between various cloud constituents, such as water vapor, water droplets, rain droplets, ice crystals, and snow, and is what we focus on in this work. In particular, we focus on accretion, which is how existing rain and snow collects more rain and snow from the water droplets and ice crystals floating around in the cloud.

Tracers (scalar quantities) evolve according to the equation

$$\frac{dQ}{dt} = \nabla \cdot (\mathbf{u}Q) + S(Q) \quad (1)$$

where Q is the tracer concentration, \mathbf{u} is the wind velocity, and $S(Q)$ is a source or sink of the tracer. Accretion is a source of rain and snow, and a sink of other cloud quantities, and so this work focuses on $S(Q)$. In order to simplify matters, we consider $\mathbf{u} = 0$.

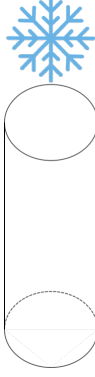


Figure 2: The cylinder model for accretion

2 Accretion Models

We describe models for how the amount of snow in a cloud affects the accretion of more snow in that cloud. We consider a falling snowflake. It sweeps out a “cylindrical” region, and thus accumulates an amount of snow. Visually, this is represented in Figure 2. The rate of the corresponding change in the specific humidity of snow is given in [1] as

$$\frac{dq_s}{dt} = \int_0^\infty n_r(r)a(r)v_{term}(r)q_c E_{cp} dr \quad (2)$$

where n_r is the size distribution, a is the surface area, v_{term} is the terminal velocity, q_c is the relevant humidity, and E_{cp} is the collision effectiveness, a dimensionless value between 0 and 1. The terminal velocity is given by the balance of gravitational, buoyancy, and drag forces. The gravitational body force is $F_g = mg$, where m is the mass and g the gravitational constant. And the buoyancy force is given by

$$F_b = m(r)\frac{\rho_a}{\rho_s}g. \quad (3)$$

We consider two different drags. Kinetic drag is given by

$$F_d = \frac{1}{2}C_d\rho_a a(r)v_{term}^2, \quad (4)$$

where C_d is the drag coefficient, ρ_a is the density of air, $a(r)$ is the surface area, and v_{term} is the terminal velocity, and Stokes drag is given by

$$F_d = 6\pi r\mu v_{term}, \quad (5)$$

where r is the radius of the sphere and μ is the dynamic viscosity. In either case we can solve the balance of forces, $F_g = F_b + F_d$, for the terminal velocity. Given a kinetic drag approximation, we find

$$v_{term}(r) = \sqrt{\frac{2m(r)g}{C_d a(r)} \left(\frac{1}{\rho_a} - \frac{1}{\rho_s} \right)}, \quad (6)$$

where $m(r)$ is the mass of the particle and ρ_s is the density of snow. Solving the balance of forces, given the Stokes drag, we have

$$v_{term}(r) = \left(1 - \frac{\rho_a}{\rho_s} \right) \frac{m(r)g}{6\pi r\mu}. \quad (7)$$

The $n_r(r)$ in (2) is given by

$$n_r(r) = N_r e^{-\lambda_r r}, \quad (8)$$

where N_r is a fixed parameter, and λ_r is a parameter depending on many others.

2.1 Stokes Drag for Non-Spherical Shapes

The given Stokes drag, equation (5), is derived from the Navier-Stokes equations, in a setting with a low Reynolds number, applied to a sphere in a fluid. This Stokes drag may work well in the model of the accretion of rain water (since rain drops are assumed to be spheres), but we'll need to adjust it for non spherical shapes. As described in [2], the Stokes drag force for a nonspherical object is given by

$$F_d = 6\pi\mu v_{term} r_n K_n, \quad (9)$$

with $K_n = 1/3 + 2r_s/(3r_n)$, representing some shape factor, and r_s being the radius of the sphere with equivalent effective surface area of the object (in our case cylinder) and r_n is the radius of the sphere with the same projected normal surface area. We note that for a sphere, $K_n = 1$, recovering the familiar expression for Stokes drag, given in (5). Also, K_n strongly depends on the shape of the particle in question. We have $r_n = r$ and the effective surface area of the cylinder given by

$$\pi r^2 + 2\pi r h = 2\pi r_s^2, \quad (10)$$

which gives us $r_s = \sqrt{\frac{r^2 + 2rh}{2}}$. Altogether, we get

$$F_d = 6\pi\mu v_{term} \left(\frac{1}{3}r + \frac{2}{3}\sqrt{\frac{r^2 + 2rh}{2}} \right). \quad (11)$$

From this, we get a terminal velocity for a cylinder of

$$v_{term}(r) = \frac{m(r)g}{2\pi\mu(r + \sqrt{2r^2 + 4rh})} \left(1 - \frac{\rho_a}{\rho_s} \right) \quad (12)$$

3 Rain Accretion

First, we model rainfall accretion, as it is considerably easier than modeling snow accretion. For a sphere, $a(r) = \pi r^2$ and v_{term} has two forms as given before so for kinetic drag, we have

$$\frac{dq_r}{dt} = N_r \pi q_r E_{cp} \sqrt{\frac{8g}{3C_d} \left(\frac{\rho_w}{\rho_a} - 1 \right)} \int_0^\infty e^{-\lambda_r r} r^{\frac{5}{2}} dr \quad (13)$$

and for Stokes drag, we have

$$\frac{dq_r}{dt} = \frac{2N_r g \pi (\rho_w - \rho_a) q_r E_{cp}}{9\mu} \int_0^\infty e^{-\lambda_r r} r^4 dr \quad (14)$$

These integrals can be written in terms of the Γ function.

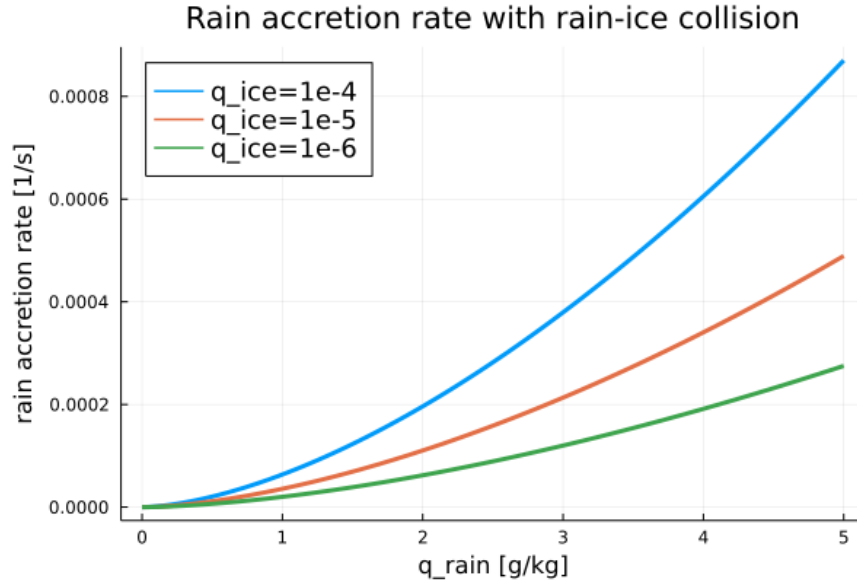


Figure 3: Rain accretion rate considering collision between rain and ice.

3.1 Computational Results

At first, we consider the rain accretion for verifying our code. The numerical calculations are done using the *Julia* programming language. We calculate the rain accretion using the following equation, which incorporates the collision between rain and ice.

$$\frac{dq_r}{dt} = \int_0^\infty \int_0^\infty \frac{1}{\rho_a} n_i(r_i) n_r(r_r) a_r(r_r) E_{ir} m_r(r_r) v_{term}(r_r) dr_i dr_r.$$

Here, the subscripts i is for ice, r is for rain and a is for air. Figure 3 shows the rain accretion rate when considering the collision between rain and ice with the probability E_{ir} . The distribution, cross-section area and terminal velocity are given in *CloudMicrophysics.jl* package of the CLiMA model [1]. The plot is showing instantaneous rain accretion rate given q_{rain} at the previous time step as a known parameter. Therefore for a given specific rain humidity, q_{rain} , we can compute the accretion rate at that given time. Now for higher ice specific humidity, we see more rain accretion. The likely cause of this behavior is the higher collision efficiency between rain and ice. This plot matches with the one in the CLiMA model for the same parameters, which verifies the code implementation.

We also consider the rain accretion rate without collision and use both kinetic and Stokes drag. The accretion rate is calculated using (2), where the integral is simplified by using the definitions for $n_r(r)$, $a(r)$, and $v_{term}(r)$. For the kinetic drag, the expanded equation for rain accretion is then given by (13), and for Stokes drag, the equation for rain accretion is given by (14). Figure 4 shows a difference between rain accretion rate between kinetic and Stokes drag. The accretion rate by Stokes drag is less by factor of 2 compared to the kinetic drag.

3.2 Tests in a Climate Model

Next, we compare kinetic and Stokes drag in CESM, the Community Earth System Model. To do this, we run an aquaplanet with modified CAM6 physics for 720 days, using a finite volume

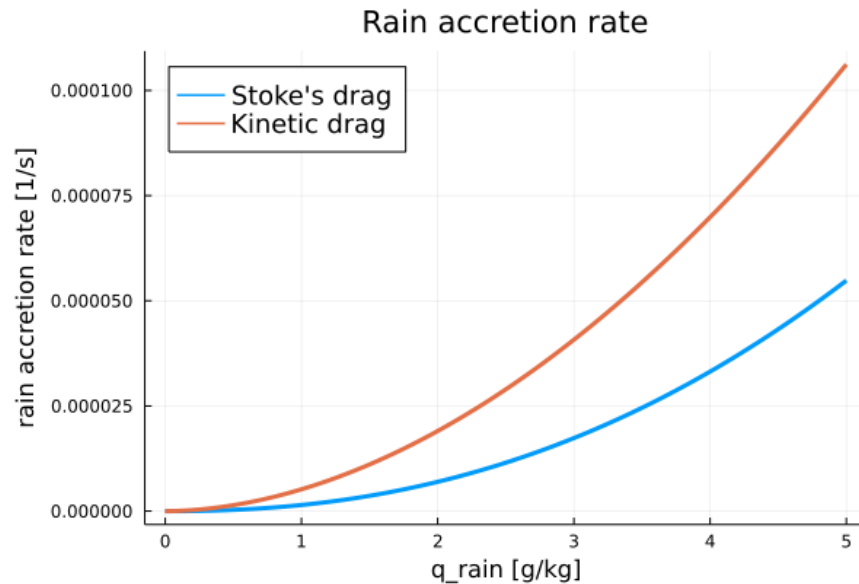


Figure 4: Comparison of Kinetic and Stokes drag for rain accretion rate.

discretization on a 1 by 1 degree grid. We modify the function `accrete_cloud_water_rain` to account for the differences between kinetic and Stokes drag.

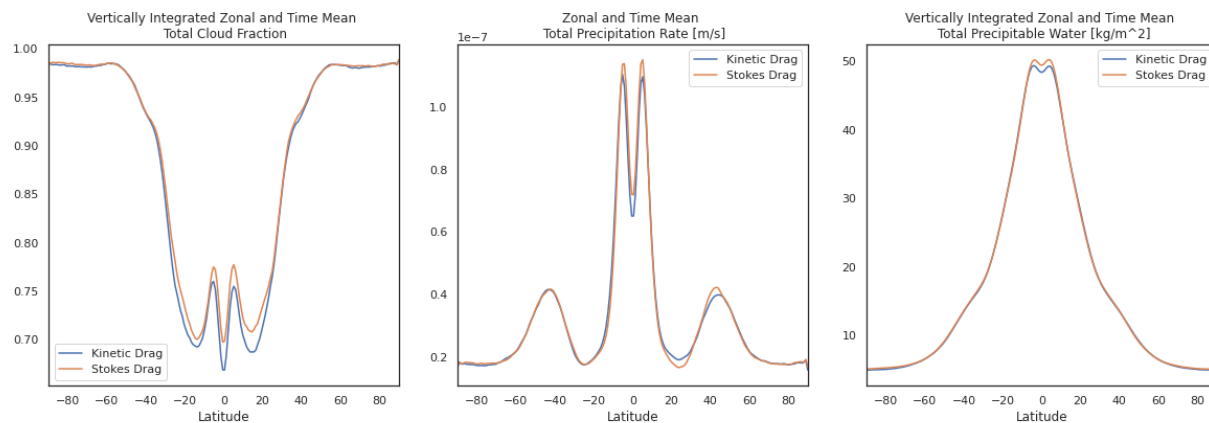


Figure 5: Comparison of (a) vertically integrated cloud fraction (b) total precipitation rate and (c) vertically integrated precipitable water for kinetic and Stokes drag.

First, we visualize the results by focusing on the vertically integrated cloud fraction, total precipitation rate, and vertically integrated precipitable water in Figure 5. We average over the last 360 days of the model run, and we also average over the longitudes, so we can see how these fields vary in the latitude. We see that Stokes drag results in higher cloud fractions, higher precipitation rates, and increased precipitable water. We think that this is sensible. Because Stokes drag results in less rain accretion, this means that less moisture is drawn out of the clouds, increasing the cloud fraction. The increased cloud fraction means that there is more moisture to draw precipitation from, and this ends up increasing the precipitation rate.

We next visualize the results with a Hovmoeller diagram in Figure 6. We average the rainfall between 5 degrees south and 5 degrees north, as this covers the latitudes where there is the most rainfall. We then plot the longitude versus the time for a 90 day period after the model has spun

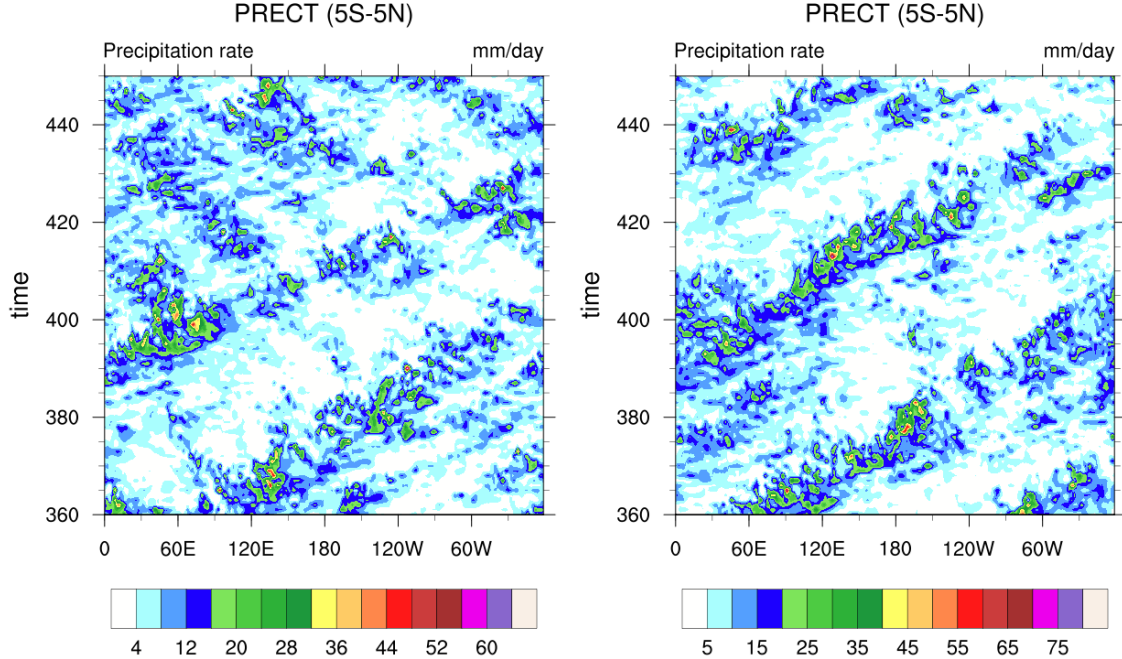


Figure 6: Hovmoeller diagrams comparing (a) kinetic drag and (b) Stokes drag.

up. The field being plotted is the precipitation rate in millimeters per day, with kinetic drag on the left and Stokes drag on the right. When looking at the Hovmoeller diagrams, it is hard to see if there are any true differences. However, one could potentially draw the conclusion that with Stokes drag, the rain is less spontaneous, and existing storms last for longer. Normally, one would expect lines of storms moving eastwards as time passes, which we see in both, but with kinetic drag, we see a number of storms that do not move to the east significantly before disappearing. In contrast, with Stokes drag, we seem to have fewer storms that last much longer. In particular, there is one rain system that lasts for close to 80 days, and circles the planet almost twice. This may be because with Stokes drag, there is less rain accretion, meaning that it is harder for the rain to deplete all the water vapor available.

4 Snowflake modeling

4.1 Simple Snowflakes

We start by modelling snowflakes as cylinders with radius r and a given height, representing the thickness of the snowflake, as seen in Figure 7. For snowflakes, the height is much smaller than the radius. We also assume that the snowflake falls without rotating such that it sweeps out a larger cylinder.

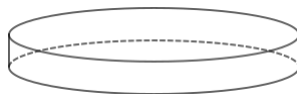


Figure 7: The cylindrical disc model for a snowflake

4.1.1 Height Proportional to Radius

We start by considering the height of the disc proportional to the radius. We have $a(r) = \pi r^2$ and $h(r) = \alpha r$ for a constant of proportionality α . First, we consider kinetic drag. Then, we have $m(r) = \pi r^2 h \rho_s = \alpha \pi r^3 \rho_s$ which gives

$$v_{term}(r) = \sqrt{\frac{2\alpha g}{C_d} \left(\frac{\rho_s}{\rho_a} - 1 \right)} r^{\frac{1}{2}}, \quad (15)$$

which gives an accretion rate

$$\frac{dq_s}{dt} = \int_0^\infty n_r(r) a(r) v_{term}(r) q_c E_{cp} dr = N_r \pi \sqrt{\frac{2\alpha g}{C_d} \left(\frac{\rho_s}{\rho_a} - 1 \right)} q_c E_{cp} \int_0^\infty e^{-\lambda r} r^{5/2} dr \quad (16)$$

$$= \frac{15}{8} N_r \pi q_c E_{cp} \sqrt{\frac{2\alpha g \pi}{C_d \lambda_r^7} \left(\frac{\rho_s}{\rho_a} - 1 \right)}. \quad (17)$$

Next, we consider Stokes drag. In this case, we have

$$v_{term}(r) = \frac{\alpha r^2 g (\rho_s - \rho_a)}{2\mu(1 + \sqrt{2 + 4\alpha})}, \quad (18)$$

so the accretion takes the form

$$\frac{dq_s}{dt} = \frac{N_r \alpha \pi g (\rho_s - \rho_a) q_c E_{cp}}{2\mu(1 + \sqrt{2 + 4\alpha})} \int_0^\infty e^{-\lambda r} r^3 dr \quad (19)$$

$$= \frac{12 N_r \pi \alpha g q_c E_{cp} (\rho_s - \rho_a)}{\mu(1 + \sqrt{2 + 4\alpha}) \lambda_r^5}. \quad (20)$$

4.1.2 Constant Height

Next, we consider snowflakes as cylinders with constant heights h_0 . First, we consider kinetic drag. Then, we have

$$v_{term}(r) = \sqrt{\frac{2h_0 g}{C_d} \left(\frac{\rho_s}{\rho_a} - 1 \right)}. \quad (21)$$

so we have accretion of the form

$$\frac{dq_s}{dt} = N_r \pi q_c E_{cp} \sqrt{\frac{2h_0 g}{C_d} \left(\frac{\rho_s}{\rho_a} - 1 \right)} \int_0^\infty e^{-\lambda r} r^2 dr \quad (22)$$

$$= \frac{2 N_r \pi q_c E_{cp}}{\lambda_r^3} \sqrt{\frac{2h_0 g}{C_d} \left(\frac{\rho_s}{\rho_a} - 1 \right)}. \quad (23)$$

Next, we consider Stokes drag. Now, we have

$$v_{term}(r) = \frac{r^2 h_0 g (\rho_s - \rho_a)}{2\mu(r + \sqrt{2r^2 + 4rh_0})}, \quad (24)$$

leading to the accretion

$$\frac{dq_s}{dt} = \frac{N_r \pi h_0 g q_c E_{cp} (\rho_s - \rho_a)}{2\mu} \int_0^\infty \frac{e^{-\lambda r} r^4}{r + \sqrt{2r^2 + 4rh_0}} dr, \quad (25)$$

which cannot be integrated analytically.

4.1.3 Constant Mass

Next, we consider snowflakes with constant mass, so $m(r) = m_0$. Then, for kinetic drag, we have

$$v_{term}(r) = \sqrt{\frac{2m_0g}{C_d\pi r^2} \left(\frac{1}{\rho_a} - \frac{1}{\rho_s} \right)}, \quad (26)$$

which we substitute into the accretion expression, giving

$$\frac{dq_s}{dt} = N_r q_c E_{cp} \sqrt{\frac{2\pi m_0 g}{C_d} \left(\frac{1}{\rho_a} - \frac{1}{\rho_s} \right)} \int_0^\infty e^{-\lambda_r r} r dr \quad (27)$$

$$= \frac{N_r q_c E_{cp}}{\lambda_r^2} \sqrt{\frac{2\pi m_0 g}{C_d} \left(\frac{1}{\rho_a} - \frac{1}{\rho_s} \right)}. \quad (28)$$

Next, for Stokes drag, we have that $h = \frac{m_0}{\pi r^2 \rho_s}$ giving

$$v_{term}(r) = \frac{m_0 g}{2\pi\mu \left(r + \sqrt{2r^2 + \frac{4m_0}{\pi r \rho_s}} \right)} \left(1 - \frac{\rho_a}{\rho_s} \right), \quad (29)$$

leading to

$$\frac{dq_s}{dt} = \frac{N_r m_0 g q_c E_{cp}}{2\mu} \left(1 - \frac{\rho_a}{\rho_s} \right) \int_0^\infty \frac{e^{-\lambda_r r} r^2}{r + \sqrt{2r^2 + \frac{4m_0}{\pi \rho_s r}}} dr, \quad (30)$$

which cannot be integrated analytically.

4.1.4 A Given Mass Distribution

Next, we integrate over mass with a given mass distribution. We assume that $n_m(m) = N_m e^{-\lambda_m m}$. The terminal velocities are as given in (4.1.3). For kinetic drag, we integrate

$$\frac{dq_s}{dt} = \int_0^\infty N_m e^{-\lambda_m m} \frac{N_r q_c E_{cp}}{\lambda_r^2} \sqrt{\frac{2\pi m g}{C_d} \left(\frac{1}{\rho_a} - \frac{1}{\rho_s} \right)} dm \quad (31)$$

$$= \frac{N_m N_r \pi q_c E_{cp}}{\lambda_r^2 \lambda_m^{\frac{3}{2}}} \sqrt{\frac{g}{2C_d} \left(\frac{1}{\rho_a} - \frac{1}{\rho_s} \right)}, \quad (32)$$

For Stokes drag, we have

$$\frac{dq_s}{dt} = \frac{N_m N_r g q_c E_{cp}}{2\mu} \int_0^\infty \int_0^\infty \frac{m e^{-\lambda_m m} r^2 e^{-\lambda_r r}}{r + \sqrt{2r^2 + \frac{4m}{\pi \rho_s r}}} dr dm. \quad (33)$$

4.2 Snowflakes with Holes

We define the area ratio β as the percent of a circle of radius r that the snowflake's area takes up, so $a(r) = \beta \pi r^2$. Then, the area of the holes is $(1 - \beta)\pi r^2$. This is seen in Figure 8. We consider the snowflake as a circle, and the area of the snowflake is β of the full circle.



Figure 8: The disc with holes model for a snowflake

4.2.1 Constant Area Ratio

For this case, we start by using the kinetic drag for now. First, we assume that $\beta = \beta_0$ is a constant. Because this doesn't affect the terminal velocity, β only affects the final accretion through the $a(r)$ term in the integral, so we have a β_0 in front of what we had before (17, 23, 28, 32):

$$\frac{d\tilde{q}_s}{dt} = \beta_0 \frac{dq_s}{dt}. \quad (34)$$

We call this the scalar approximation.

4.2.2 Normally Distributed Area Ratio

Next, we consider a distribution for the area ratio β . Based on [5], we say that β is normally distributed with $\mu = 0.64$ and $\sigma = 0.173$. Because β ranges from 0 to 1, we multiply by a constant so that $n_\beta(\beta)$ integrates to 1. Then, we have that

$$n_\beta(\beta) = \frac{N_\beta}{\sqrt{2\pi(0.173)^2}} e^{-\frac{(\beta-0.64)^2}{2(0.173)^2}} \quad (35)$$

with N_β chosen such that

$$\int_0^1 n_\beta(\beta) d\beta = 1. \quad (36)$$

Then, we have that

$$\frac{dq_s}{dt} = \int_0^1 n_\beta(\beta) \beta d\beta \int_0^\infty n(r) a(r) v_{term}(r) q_c E_{cp} dr. \quad (37)$$

We have that $N_\beta \approx 2.45$. We note that only the first two terms depend on β so we can integrate this separately, and we have that

$$\int_0^1 n_\beta(\beta) \beta d\beta \approx 0.632. \quad (38)$$

4.2.3 Area Ratio as a Function of Radius

Next, we consider β as a function of r . We take

$$\beta(r) = \beta_{\min} + (1 - \beta_{\min}) e^{-\lambda_\beta r}. \quad (39)$$

The idea is that as snowflakes become bigger, they become emptier, down to some baseline. If a snowflake is too empty, it will break apart, which is where β_{\min} comes from. Then, we have that

$$a(r) = \beta(r) \pi r^2. \quad (40)$$

Now, we have kinetic drag with $h = \alpha r$. Then

$$m(r) = \beta(r)\alpha\pi r^3\rho_s. \quad (41)$$

Next, we have

$$\frac{dq_s}{dt} = \int_0^\infty N_r e^{-\lambda_r r} (\beta_{\min} + (1 - \beta_{\min})e^{-\lambda_\beta r}) \sqrt{\frac{2\alpha r g}{C_d} \left(\frac{1}{\rho_a} - \frac{1}{\rho_s} \right)} q_c E_{cp} dr, \quad (42)$$

which gives

$$\frac{dq_s}{dt} = \frac{15N_r q_c E_{cp}}{8} \sqrt{\frac{2\pi^3 \alpha g}{C_d} \left(\frac{1}{\rho_a} - \frac{1}{\rho_s} \right)} \left(\frac{1}{(\lambda_r + \lambda_\beta)^{\frac{7}{2}}} + \beta_{\min} \left(\frac{1}{\lambda_r^{\frac{7}{2}}} - \frac{1}{(\lambda_r + \lambda_\beta)^{\frac{7}{2}}} \right) \right). \quad (43)$$

We note that because of how kinetic drag affects the terminal velocity, the v_{term} terms here are the same as those given in (4.1.1, 4.1.2, 4.1.3). Next, we take $h = h_0$. Then, we have that

$$\frac{dq_s}{dt} = N_r \pi q_c E_{cp} \sqrt{\frac{2\pi^3 h_0 g}{C_d} \left(\frac{1}{\rho_a} - \frac{1}{\rho_s} \right)} \left(\frac{\beta_{\min}}{\lambda_\beta - \frac{\beta_{\min}-1}{(\lambda_r + \lambda_\beta)^3}} \right). \quad (44)$$

Next, we have a constant mass m_0 . Then, we have that

$$\frac{dq_s}{dt} = N_r \pi q_c E_{cp} \sqrt{\frac{2m_0 g}{C_d \pi} \left(\frac{1}{\rho_a} - \frac{1}{\rho_s} \right)} \int_0^\infty \frac{e^{-\lambda_r r} r}{\sqrt{\beta(r)}} dr. \quad (45)$$

This cannot be integrated analytically. Next, we integrate over the mass distribution, giving

$$\frac{dq_s}{dt} = N_m N_r q_c E_{cp} \pi \sqrt{\frac{g}{2C_d \lambda_m^3}} \int_0^\infty \frac{e^{-\lambda_r r} r}{\sqrt{\beta(r)}} dr. \quad (46)$$

4.2.4 Stokes Drag with Holes

How do we deal with Stokes drag with holes? Assume that we have k identical holes, each with radius r_k . Then, the normal projection surface area is $\beta\pi r^2$ which equals πr_n^2 so $r_n = \sqrt{\beta}r$. Additionally, because we know that

$$\pi r^2 - k\pi r_k^2 = \beta\pi r^2, \quad (47)$$

so $r_k = \sqrt{\frac{1-\beta}{k}}r$. Then, we find that

$$r_s = \sqrt{(1 + \sqrt{k(1-\beta)})(rh) + \frac{\beta}{2}r^2}. \quad (48)$$

Now, we have that $F_d = 6\pi\mu v_{term} \left(\frac{r_n}{3} + \frac{2r_s}{3} \right)$, giving

$$F_d = 2\pi\mu v_{term} \left(\sqrt{\beta}r + 2\sqrt{(1 + \sqrt{k(1-\beta)})(rh) + \frac{\beta}{2}r^2} \right), \quad (49)$$

and from this, we find the terminal velocity

$$v_{term} = \frac{m(r)g}{2\pi\mu(\sqrt{\beta}r + 2\sqrt{(1 + \sqrt{k(1-\beta)})(rh) + \frac{\beta}{2}r^2})}. \quad (50)$$

At this point, one could assume a distribution on the number of holes and perform similar analysis to what we have done previously. We refrain from such activities at this time.

4.3 Snowflakes as Fractals

Instead of assuming that $a(r) \sim r^2$, we assume that $a(r) \sim r^d$, where $d \in [1, 2]$. When $d = 1$, the snowflake is a line, and when $d = 2$, the snowflake is fully two dimensional.

4.3.1 A Fixed Dimension

Consider $a(r) = Cr^d$, where C is some scaling constant and d is fixed. First, we consider a constant height $h = h_0$. For this, we get a terminal velocity of

$$v_{term}(r) = \sqrt{\frac{2h_0g}{C_d} \left(\frac{\rho_s}{\rho_a} - 1 \right)}, \quad (51)$$

which gives an integral

$$\frac{dq_s}{dt} = N_r C q_c E_{cp} \sqrt{\frac{2h_0g}{C_d} \left(\frac{\rho_s}{\rho_a} - 1 \right)} \int_0^\infty e^{-\lambda_r r} r^d dr \quad (52)$$

$$= \frac{N_r C q_c E_{cp} \Gamma(d+1)}{\lambda_r^{d+1}} \sqrt{\frac{2h_0g}{C_d} \left(\frac{\rho_s}{\rho_a} - 1 \right)}. \quad (53)$$

Next, we consider $h = \alpha r$, which gives a terminal velocity of

$$v_{term}(r) = \sqrt{\frac{2r\alpha g}{C_d} \left(\frac{\rho_s}{\rho_a} - 1 \right)}, \quad (54)$$

which gives an integral

$$\frac{dq_s}{dt} = N_r C \sqrt{\frac{2\alpha g}{C_d} \left(\frac{\rho_s}{\rho_a} - 1 \right)} q_c E_{cp} \int_0^\infty e^{-\lambda_r r} r^{d+\frac{1}{2}} dr \quad (55)$$

$$= \frac{N_r C q_c E_{cp} \Gamma(d + \frac{3}{2})}{\lambda_r^{d+\frac{3}{2}}} \sqrt{\frac{2\alpha g}{C_d} \left(\frac{\rho_s}{\rho_a} - 1 \right)}. \quad (56)$$

Next, we consider $m = m_0$ which gives a kinetic energy of

$$v_{term}(r) = \sqrt{\frac{2m_0g}{C_d C r^d} \left(\frac{1}{\rho_a} - \frac{1}{\rho_s} \right)}, \quad (57)$$

which gives the integral

$$\frac{dq_s}{dt} = N_r q_c E_{cp} \sqrt{\frac{2Cm_0g}{C_d} \left(\frac{1}{\rho_a} - \frac{1}{\rho_s} \right)} \int_0^\infty e^{-\lambda_r r} r^{\frac{d}{2}} dr \quad (58)$$

$$= \frac{N_r q_c E_{cp} \Gamma(\frac{d}{2} + 1)}{\lambda_r^{\frac{d}{2}+1}} \sqrt{\frac{2Cm_0g}{C_d} \left(\frac{1}{\rho_a} - \frac{1}{\rho_s} \right)}. \quad (59)$$

Next, we integrate this over a mass distribution, which gives

$$\frac{dq_s}{dt} = \frac{N_r N_m q_c E_{cp} \Gamma(\frac{d}{2} + 1)}{\lambda_r^{\frac{d}{2}+1}} \sqrt{\frac{2Cg}{C_d} \left(\frac{1}{\rho_a} - \frac{1}{\rho_s} \right)} \int_0^\infty e^{-\lambda_m m} \sqrt{m} dm \quad (60)$$

$$= \frac{N_r N_m q_c E_{cp} \Gamma(\frac{d}{2} + 1)}{\lambda_r^{\frac{d}{2}+1} \lambda_m^{\frac{3}{2}}} \sqrt{\frac{Cg\pi}{2C_d} \left(\frac{1}{\rho_a} - \frac{1}{\rho_s} \right)}. \quad (61)$$

4.3.2 Varying Fractal Dimension

Now, instead of fixing d , we assume that d is uniformly distributed between 1 and 2. We would then integrate the expressions (53, 56, 59, 61) with respect to d from 1 to 2. None of the integrals can be computed analytically.

4.3.3 Fractal Stokes Drag

Assume that $h(r) \ll r$, as noted in [3]. In this case, when working with the Stokes drag, the effective surface area and the normal projected surface area are the same because there are no sides. Then, if we have the surface area $a(r) = Cr^d$, we have that $\pi r_n^2 = Cr^d$ and $2\pi r_s^2 = Cr^d$ giving us $r_n = \sqrt{\frac{C}{\pi}r^{\frac{d}{2}}}$ and $r_s = \sqrt{\frac{C}{2\pi}r^{\frac{d}{2}}}$. Then, we have that

$$r_n K_n = \frac{r_n}{3} + \frac{2r_s}{3} = \sqrt{\frac{C}{\pi}} \frac{(1 + \sqrt{2})r^{\frac{d}{2}}}{3}, \quad (62)$$

leading to Stokes drag of the form

$$F_d = 6\pi\mu v_{term} \frac{(1 + \sqrt{2})r^{\frac{d}{2}}}{3} \sqrt{\frac{C}{\pi}}. \quad (63)$$

Now, we find that the terminal velocity is of the form

$$v_{term} = \frac{m(r)g}{2\mu(1 + \sqrt{2})\sqrt{a(r)}\pi} \left(1 - \frac{\rho_a}{\rho_s}\right). \quad (64)$$

4.4 Hexagonal Snowflakes

We also try using hexagonal plates as an approximation of a snowflake, as this is one shape in which snowflakes do naturally form (see [4], Fig. 9).

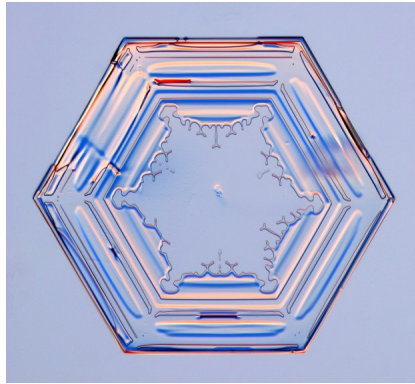


Figure 9: A hexagonal snowflake

Because the kinetic drag force does not depend on the shape of our object, the balance of forces leads us to the same terminal velocity as in the cylindrical case given in (21). The projected area of a hexagonal plate defined by the radius of the circle in which it is inscribed is $a(r) = \frac{3}{2}\sqrt{3}r^2$. This terminal velocity, $v_{term}(r)$, and projected area, $a(r)$, will define the integral in (2), yielding the source term we want in this case.

We can also do the Stokes drag analysis on the hexagonal plate. We do this with a fixed h_0 , but alternative cases for describing snowflake thickness follow quickly. As we've done previously, the comparison of effective surface areas

$$\frac{3}{2}\sqrt{3}r^2 + 6rh_0 = 2\pi r_s^2, \quad (65)$$

yields

$$r_s = \frac{\sqrt{12rh_0 + 3\sqrt{3}r^2}}{2}. \quad (66)$$

Similarly, comparing the projected surface areas of a sphere and the hexagonal plate (a circle and a hexagon) yields

$$r_n = \sqrt{\frac{3\sqrt{3}}{2\pi}}r. \quad (67)$$

Thus the drag force on a hexagonal plate is

$$F_d = 2\pi\mu v_{term}(r_n + 2r_s) \quad (68)$$

$$= \pi\mu v_{term} \left(\sqrt{\frac{3\sqrt{3}}{2\pi}}r + \sqrt{12rh_0 + 3\sqrt{3}r^2} \right). \quad (69)$$

From the balancing of F_b , F_g , and F_d we find

$$v_{term} = \frac{\frac{3}{2}\sqrt{3}r^2 h_0 \rho_s g \left(1 - \frac{\rho_a}{\rho_s}\right)}{\pi\mu \sqrt{\frac{3\sqrt{3}}{2\pi}}r + \sqrt{12rh_0 + 3\sqrt{3}r^2}}. \quad (70)$$

Again, in combination with the projected area for a hexagonal plate, $a(r) = \frac{3}{2}\sqrt{3}r^2$, we can find the form of (2) in this case. Again, this has no analytical solution.

4.5 Snowflakes with Varying Angles

If a snowflake is falling at an angle θ , the normal projected surface area will be

$$\tilde{a}(r) = a(r) \cos \theta, \quad (71)$$

so as a snowflake becomes more tilted, it will sweep out a smaller cylinder. This can be seen in Figure 10.

4.5.1 A Fixed Angle

We assume that all snowflakes fall at the same angle θ_0 . Then, we have a kinetic drag of the form

$$v_{term}(r) = \sqrt{\frac{2m(r)g}{C_d a(r) \cos \theta_0} \left(\frac{1}{\rho_a} - \frac{1}{\rho_s} \right)}. \quad (72)$$

In this case, all that happens is we get equations (53, 56, 59, 61) but with an additional factor of $(\cos \theta_0)^{-\frac{1}{2}}$ in front.

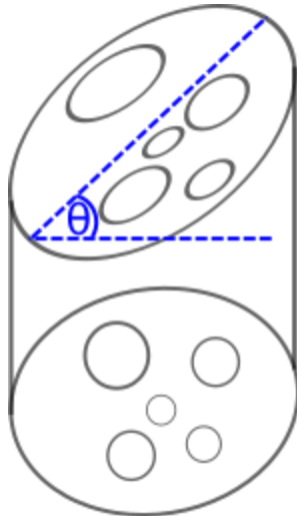


Figure 10: A snowflake falling at an angle

4.5.2 Varying Angles

We assume that the angles are normally distributed between 0 and $\frac{\pi}{2}$. We can restrict to this instead of varying between 0 and 2π by symmetry. In this case, we would get a factor of

$$\frac{2}{\pi} \int_0^{\frac{\pi}{2}} \sqrt{\cos \theta} d\theta = \Gamma\left(\frac{3}{4}\right)^2 \left(\frac{2}{\pi}\right)^{\frac{3}{2}} \approx 0.763. \quad (73)$$

5 Computational Results

We model snow accretion rate numerically using various models explained in Section 4.

5.1 Simple Snowflakes

We first consider the snowflake as a disc with 1) a height that is proportional to the radius and 2) a constant height. Figure 11 shows the snow accretion rate using a height that is proportional to the radius with constant of proportionality α . We calculate the accretion rate for three different cases of α , which means varying the thickness of a snowflake. We see higher accretion rate for smaller α . Figure 12 explains the accretion rate using a constant height of the disc, which means constant snowflake thickness. In this case, the plots suggest that the accretion rate is higher for thicker snowflakes. This is contradictory compared to the previous case. This behavior is probably due to a difference in the nature of the integral function.

Also, both cases are shown with kinetic and Stokes drag. The difference in magnitude between these two drag forces for both cases is of order 10. The Stokes drag is derived from the Navier-Stokes equations using a small Reynolds number limits. The Reynolds number for the snowflakes is of order 1 because the length scale of the snowflake is much smaller. Therefore, for relatively small size of snowflakes, the Stokes drag might be reasonable to use. However, as the snowflake size increases, it not only increases the length scale but also the terminal velocity. This ultimately increases the Reynolds number. In those case, the kinetic drag might serve well for the accretion rate calculation.

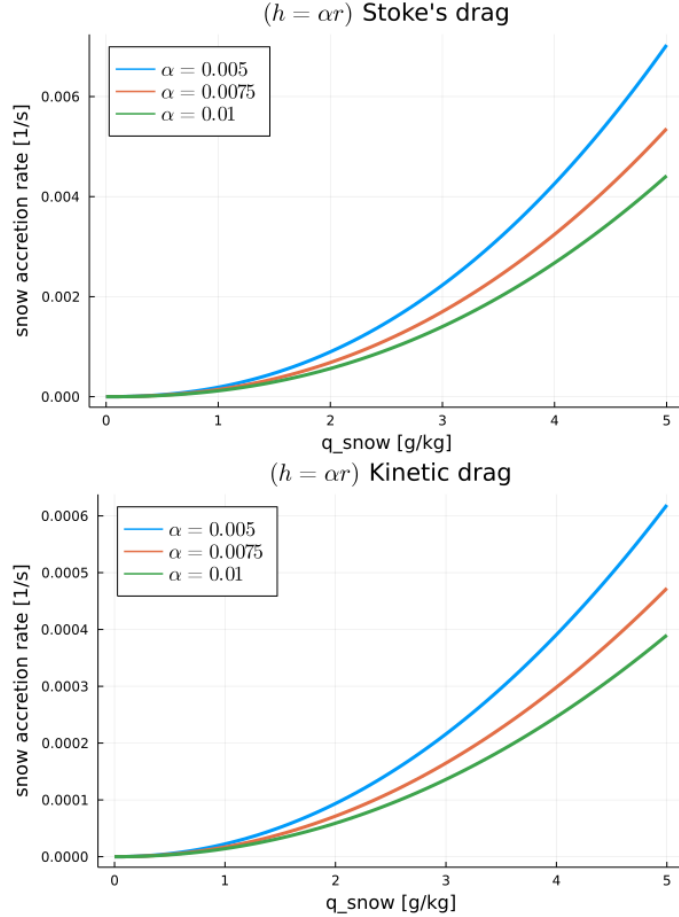


Figure 11: Snow accretion rate for(a) Stokes drag and (b) Kinetic drag using the disc model with the height proportional to the radius.

Now, we consider the cases with 1) a constant mass and 2) mass distribution. For the case of constant mass we use formula we use (27) for the kinetic drag and (30) for Stokes drag. In the case of Stokes drag we utilized the QuadGK package to numerically approximate the integral in (30). We consider three cases of fixed mass $m_0 = 10^{-6}$, 5×10^{-6} , 10^{-5} kg. These results are shown in Figure 13. We see that mass and accretion rate have an inverse relationship. We believe this is because a snowflake with higher mass will have higher terminal velocity as seen in (26) and (29). Since the collision efficiency between cloud ice and snow is so low, a faster moving snowflake will accrete at a slower rate.

As in section 4.1.4 we can consider a distribution of the mass of snowflakes to refine the accretion rate. In Eq(33) we consider an exponential distribution, however, further literature review is needed to determine if this is an accurate assumption, and to determine realistic parameters for the distribution. We tested several values of λ_m in our code but our results did not seem physically realistic.

5.2 Snow with holes

The case with snow with holes involves a distribution for $\beta(r)$ that comes with two free parameters; β_{min} and λ_β . Here, β_{min} is a minimum fraction of filled surface area of the disc that is equivalent

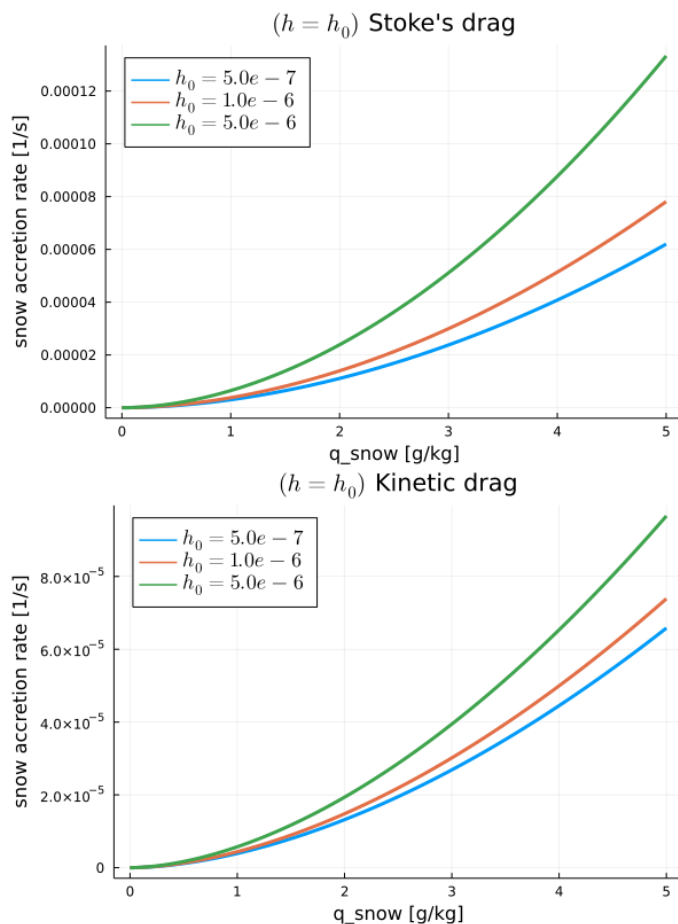


Figure 12: Snow accretion rate for (a) Stokes drag and (b) Kinetic drag using the disc model with a constant height.

to the snow flake are. We use this distribution for surface area and also mass. However, the free parameters involved in the distribution need to be evaluated using some experimental studies. We could not fit more literature study in the time frame of this workshop but this is something to be considered in detailed in future.

5.3 Hexagonal shape model

A snowflake model using a hexagonal shape is also explored numerically. This case can be compared with the disc assumption because of the difference in the cross section area. Figure 14 shows the snow accretion rate using kinetic drag and considering the constant height case. The plot is very similar to the one with the disc assumption but with a small scaling. This is the ratio of the areas between a circle and a hexagon.

5.4 Fractal model

A snowflake model using a fractal dimension is explored numerically in this section. This case can be compared with the disc assumption because of the difference in the cross section area. Figure 14 shows the snow accretion rate using kinetic drag and considering the constant height case. The

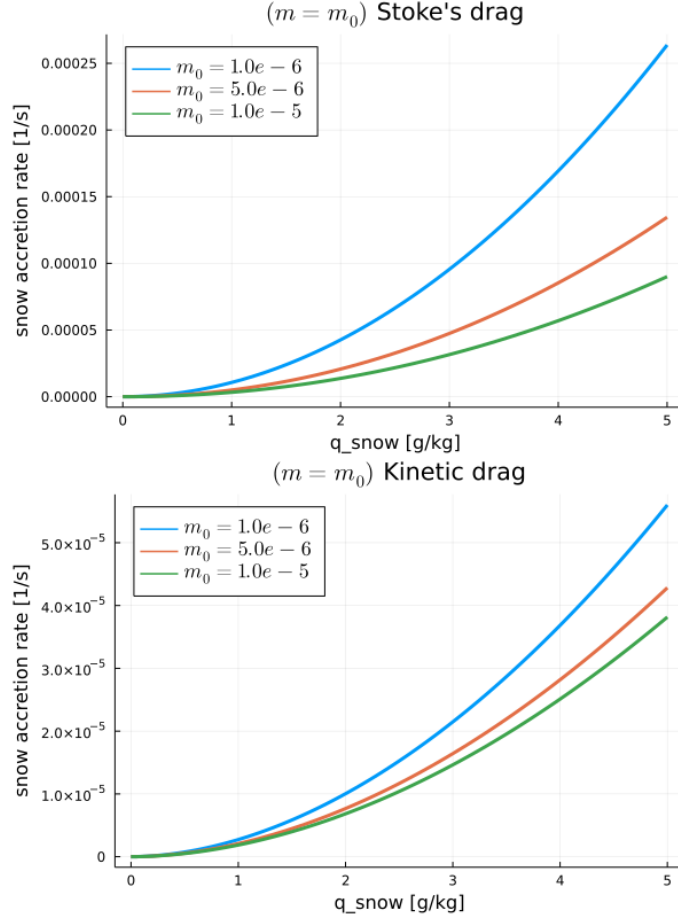


Figure 13: Snow accretion rate for (a) Stokes drag and (b) Kinetic drag using the disc model with a constant mass.

plot is very similar to the one with the disc assumption but with a small scaling. This is the ratio of the areas between a circle and a hexagon.

6 Conclusion

In this work, we considered the cylinder model for snow accretion in first moment cloud microphysics calculations. We started with a simple cylindrical disc snowflake, varying both the height and mass, before we considered snowflakes with holes, snowflakes as fractals, hexagonal snowflakes, and snowflakes falling at varying angles. We considered all of these with both kinetic and Stokes drag, and saw very different behavior between them. We implemented many of these snowflake models and evaluated them numerically as well. However, we were unable to implement some of them because of time constraints.

There remains further work to be done. All of the integrals used are indefinite integrals from 0 to ∞ , which is unphysical. We could instead use definite integrals. We could also consider time dependent parameters. For example, snowflakes fall according to a back and forth (leaf-like) pattern so they do not quite sweep out a cylinder. Even if we do not consider a fully time dependent model, we would like to see if we can model this effect in some averaged way. We could also consider a more detailed hole model, or consider heterogeneous snow. Snow takes on a wide variety of shapes, sizes,

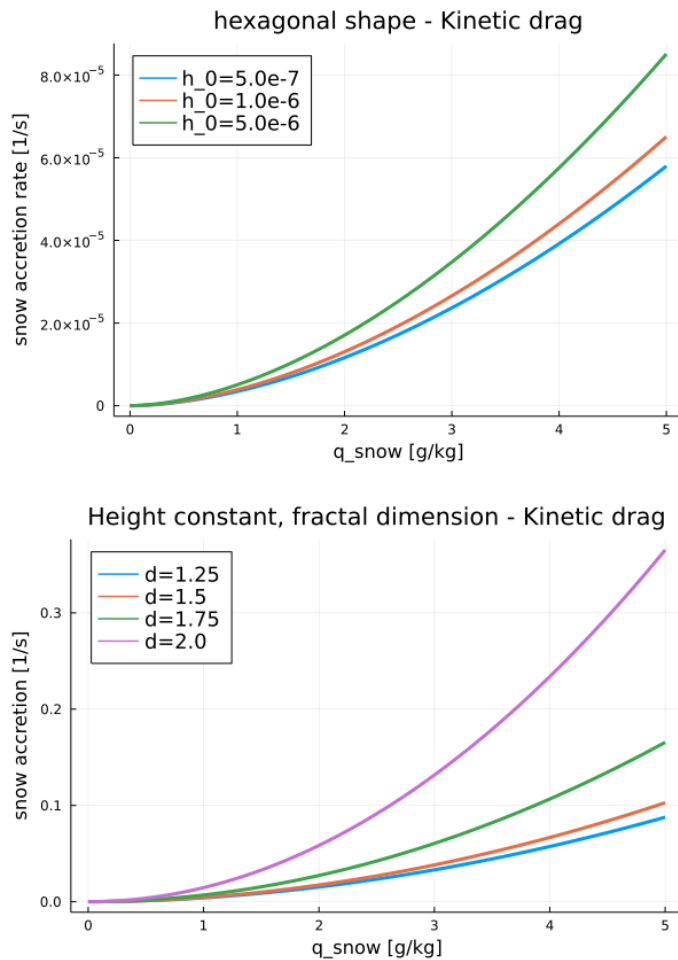


Figure 14: Snow accretion rate for (a) Hexagonal shape model and (b) fractal dimension with a constant height

and morphologies, and all of them interact differently with their surroundings. Additionally, as snow falls, snowflakes can clump together. This adds a number of complications. For example, as snowflakes clump, they likely clump in three dimensions, giving a fractal dimension $d \in [1, 3]$. We would also like to consider a potential intermediate domain where kinetic drag and Stokes drag approach each other in some limit.

7 Acknowledgements

We thank Dr. Edwards and Dr. Fok for running the camp and helpful commentary, Susan Dziombak for coordinating, Anna Jaruga for providing insightful answers to our questions, the University of Delaware for hosting us, and the NSF and SIAM for funding this camp.

References

- [1] CLIMA, *CloudMicrophysics.jl package documentation*. <https://clima.github.io/CloudMicrophysics.jl/dev/>.
- [2] D. LEITH, *Drag on nonspherical objects*, *Aerosol Science and Technology*, 6 (1987), pp. 153–161.
- [3] K. G. LIBBRECHT, *Physical dynamics of ice crystal growth*, *Annual Review of Materials Research*, 47 (2017), pp. 271–295.
- [4] S. Y. MATROSOV ET AL, *Estimation of ice hydrometeor types and shapes from radar polarization measurements*, *Journal of Atmospheric and Oceanic Technology*, 13 (1996), pp. 85–96.
- [5] J. TIIRA, D. N. MOISSEEV, A. VON LERBER, D. ORI, A. TOKAY, L. F. BLIVEN, AND W. PETERSEN, *Ensemble mean density and its connection to other microphysical properties of falling snow as observed in southern finland*, *Atmospheric Measurement Techniques*, 9 (2016), pp. 4825–4841.